Cell, Volume *136*

Supplemental Data

The Ste5 Scaffold Directs Mating Signaling by Catalytically Unlocking the Fus3 MAP Kinase for Activation

Matthew Good, Grace Tang, Julie Singleton, Attila Remenyi, and Wendell A. Lim

SUPPLEMENTAL EXPERIMENTAL PROCEDURES

Protein Expression and Purification (expanded)

Constructs expressing recombinant proteins were generated by PCR; mutant variants were generated by two-step PCR, using internal mutagenic primers. Fus3 and Fus3-K42R were expressed at 18^{o}C in Rosetta(DE3)pLysS E.coli cells (Novagen) using the pBH4 vector to generate an N-terminal His6-tagged, TEV-cleavable protein. Purification was carried out as described previously (Remenyi et al., 2005). Kss1 and Ste7 variants were expressed in *Spodoptera frugiperda* (SF9) cells, using the Bac-to-Bac Baculoviral Expression System (Invitrogen), at 27^{o}C. Kss1 was expressed with an N-terminal TEV-cleavable His6 tag, while Ste7 was expressed with N-terminal TEV cleavable GST, and C-terminal His6 tag. Kss1 purification was similar to Fus3, while GST-Ste7 was purified by successive affinity columns, Ni-NTA (Qiagen) and Glutathione Agarose (Sigma). Ste5 variant proteins were expressed at 18^{o}C in Rosetta(DE3)pLysS E.coli cells as either GST-fusions (pETARA vector) or MBP-

fusions (pMBP-MG vector, modified NEB pMAL vector). Proteins were purified using Ni-NTA, Glutathione Agarose beads or Amylose resin (NEB), and dialyzed into 'Standard Buffer' (150mM NaCl, 25mM Tris pH8, 10% Glycerol, 2mM DTT). The Ste5-ms protein used for crystallography was expressed as an N-terminal TEV-cleavable His6 fusion (pBH4 vector) in Rosetta cells, and purified in manner similar to Fus3 (Ni-Nta, TEV cleavage, ResourceQ ion exchange)

Structure Determination (expanded)

All diffraction data was processed using HKL2000 (Otwinowski and Minor, 1997). Heavy atoms positions were found by SOLVE (Terwilliger and Berendzen, 1999) and initial solvent flattened maps were generated RESOLVE (Terwilliger, 2003). An preliminary automated model was built using ArpWarp6.0 (Morris et al., 2003). Additional model building was done manually with Coot (Emsley and Cowtan, 2004), and TLS refinement was done using Refmac5 (Murshudov et al., 1997) and Phenix (Adams et al., 2002).

The cryopreservant for x-ray data collection (not mentioned in the main methods) was made by mixing 12% PEG 3350 and 34% Glycerol 1:1 (vol:vol) with hanging drop solution).

Supplemental Figure 1 - Anti-phospho MAPK western blot measures Fus3 and Kss1 phosphorylation

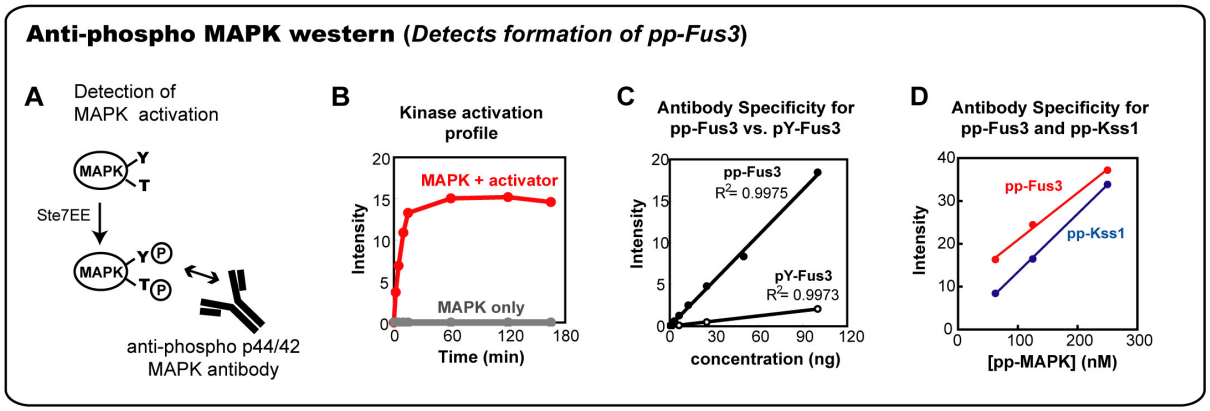

Supp. 1: Anti-phospho MAPK western blot kinase assay. (A,B) In vitro western detects dual phosphorylation of Fus3's or Kss1's activation loop using anti-phospho p44/42 MAPK antibody (Cell Signaling Technology, #9101). (C) Anti-phospho MAPK western is linear from intensity 0.1 to 40. Antibody preferentially recognizes Fus3 dually phosphorylated on Thr180 and Tyr182 (pp-Fus3) compared to Fus3 monophosphorylated on Tyr182 (pY-Fus3): it is 10-fold more specific for pp-Fus3 vs. pY-Fus3. (D) Antibody has equal preference for dually phoshorylated Fus3 and Kss1. pp-Fus3 and pp-Kss1 samples were generated by prior incubation with Ste7EE until phospho-incorporation reached a plateau.

Supplemental Figure 2 - Trulight kinase assay monitors kinase activity

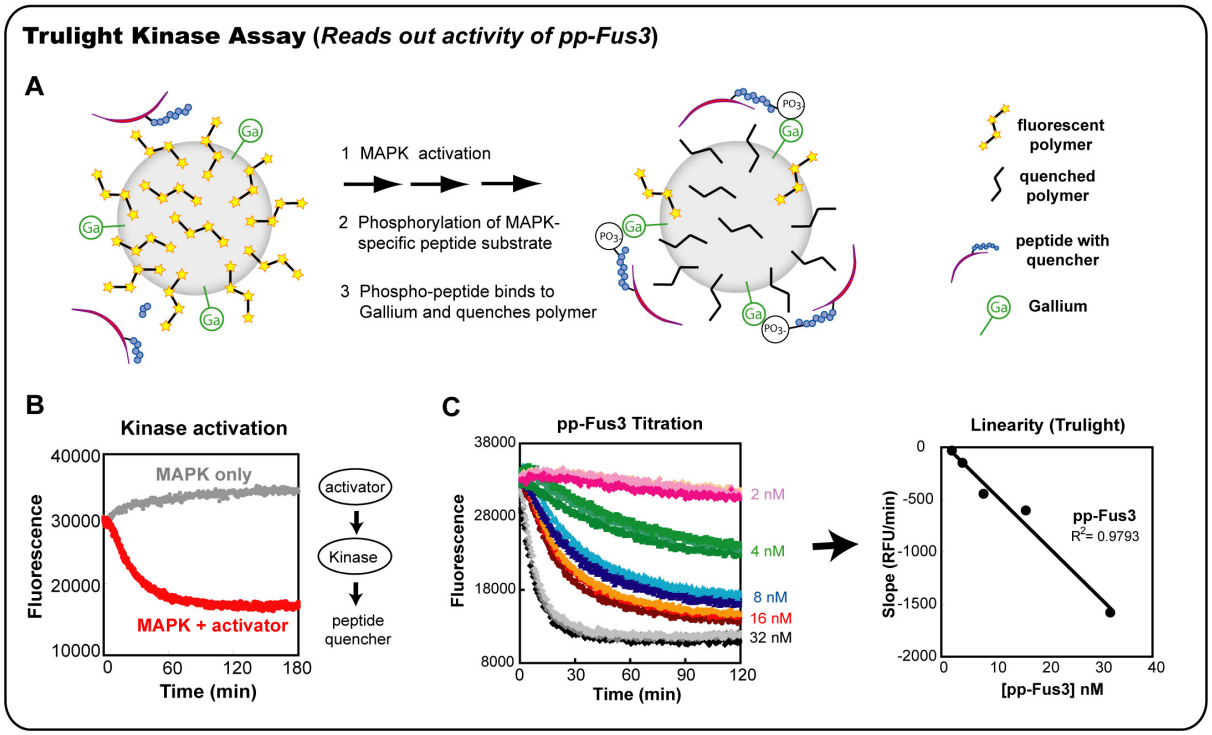

Supp. 2: (A) Trulight assay reads out activity of Fus3 and Kss1 MAP kinases. Kinases are phosphorylated by Ste7 to turn them on. Active MAPK then phosphorylates a labeled MAPK-specfic peptide (LVEPLTPSGEAPNQK) which, when phosphorylated, binds to Gallium on the sensor bead and quenches the fluorescent polymers on the bead. (B) Activity is monitored by the slope of fluorescence quenching. A steeper slope correlates with higher activity. (C) Triplicate curves show the slopes generated by titration of dually-phosphorylated Fus3 (pp-Fus3). Assay has a 65-fold linear range of activity.

Supplemental Figure 3 - Ste5 domain architecture, domain identification, and conservation

A

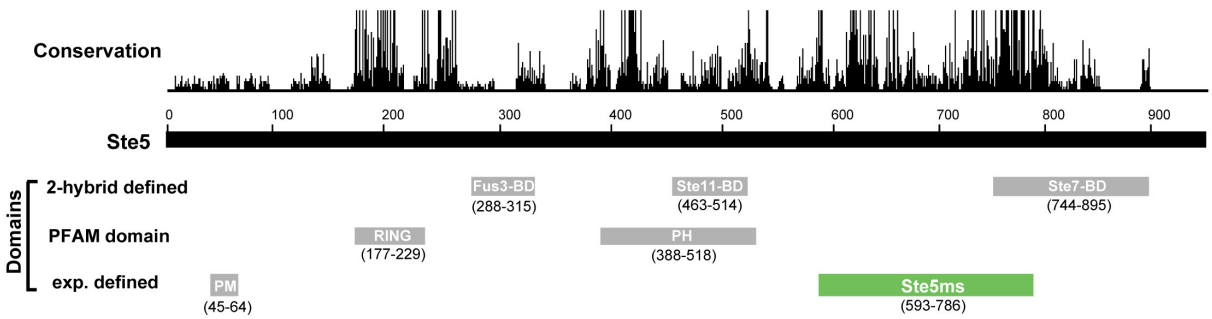

B

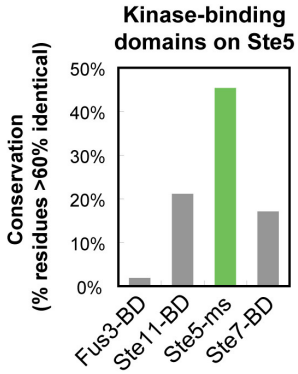

Supp. 3: (A) Domain architecture of Ste5ms and conservation of across the five currently known Ste5 fungal homologs (from *Saccharomyces cerevisiae* (*Scer*), *Vanderwaltozyma polysporus* (*Vpol*), *Ashbya gossypii* (*Agos*), *Candida glabrata* (*Cgla*), and *Kluyveromyces lactis* (*Klac*). Ste5 domains were defined previously by 2-hybrid, sequence homology (eg. PFAM) or experimentally. The Ste5-ms domain was identified in this paper. (B) Ste5-ms is the most conserved of the four domains on *Scer* Ste5 known to bind to MAPK cascade kinases - highlighting its evolutionary importance. (C) Multiple sequence alignment of Ste5-ms homologs from five fungi (*Scer, Vpol, Agos, Cgla, Klac*). 100% identical regions are colored black, highly conserved (60-80% identical) residues in light and dark gray.

Conclusion: The Ste5-ms domain is the most conserved kinase-binding region on the Ste5 scaffold.

C **Alignment of Ste5-ms homologs**

```
scer_ms   593  LTTISSILSLKREKPDNLAIILQIDFTKLKEE--DSLIVVYNSLKALTIKFARLQFCFVD  650
vpol_ms   598  MTSVSSILSLKRERPEGIVIILQLDFRKLKD---DSYIIIYNSLQALVTKYPNLIYCTVD  654
klac_ms   498  LTSISSILSIKRATPNELNLVLQLDKRKTNE---DNIVSIKNVILALTWKFSTFNCCIVD  554
agos_ms   513  RASINSILSLKRRHPDELCLFFQIDTAKVQA---VDYKILANTCKAILWKFNTAKVALAD  569
cgla_ms   370  NTITSSVLSIKKEKPSDILLLIQIDEQKITDQKDQIKQVIKNTLMALKLKYPEYFLVILS  429

scer_ms   651  RNNYVLDYGSVLHKIDSLDSISN-LKSKSSSTQFSPIWLKNTLY--PENIHEHLGIVAVS  707
vpol_ms   655  ADGFVVQYGQASKDILNLQSIYK-MNKPNAGIKFSPTWLKNTIY--PLGITSSLGIAILS  711
klac_ms   555  VEGMVINCGTAND---VLNSLAGPIKSNGNQ-PFSPDLLHQLWYRQKQKICKNVGVVVLS  610
agos_ms   570  SNGGIVTMSLLKDFIPIFSSIDHILRRHETRRKLSPNLVYRHFYGKER--LKNVGVCIIS  627
cgla_ms   430  ATGEVLLMDSIDRLNLDNQLLSG--EEPKNPFRLEISSIRTHVYG--TSILENLAIVAVS  485

scer_ms   708  NSNMEAKKSILFQDYRCFTSFGRRRPNELKIKVGYLNVDYSDKIDELVEASSWTFVLETL  767
vpol_ms   712  NGSMEEARSCLLMDYKIFASPGRRHANELKIKVGYLNSDYSDKITELVEIGTWAFMLEAL  771
klac_ms   611  NSSMENGKSCLFSDYRIFADAGKRHPNELKIKVGFLNVDYSDNIKELVEIQDWNELLEAV  670
agos_ms   628  NSAMQYGKSLLLMDYSAFCNIGKKRPNELKVKVGYLNTDYSDQVFELVETGGWGDVLEVV  687
cgla_ms   486  NSAMVETTSILFKNFSPLISKGRLRPNEIRIKVGYSNNDYSDVVSELVEIESWDYLLEAL  545

scer_ms   768  CYSFGLSFDEHDDDDEEDN----                                        786
vpol_ms   772  CYSFSLSFEDDDDDEDEDDAGDD                                        794
klac_ms   671  AYSFNLSFDDDLDSSD-------                                        686
agos_ms   688  CYSFNMAFGQDDYSDDDETED--                                        708
cgla_ms   546  CHTFSLDYDDD-----------                                         556
```

Supplemental Figure 4 - Analyzing kinetic data from anti-phospho MAPK western blots

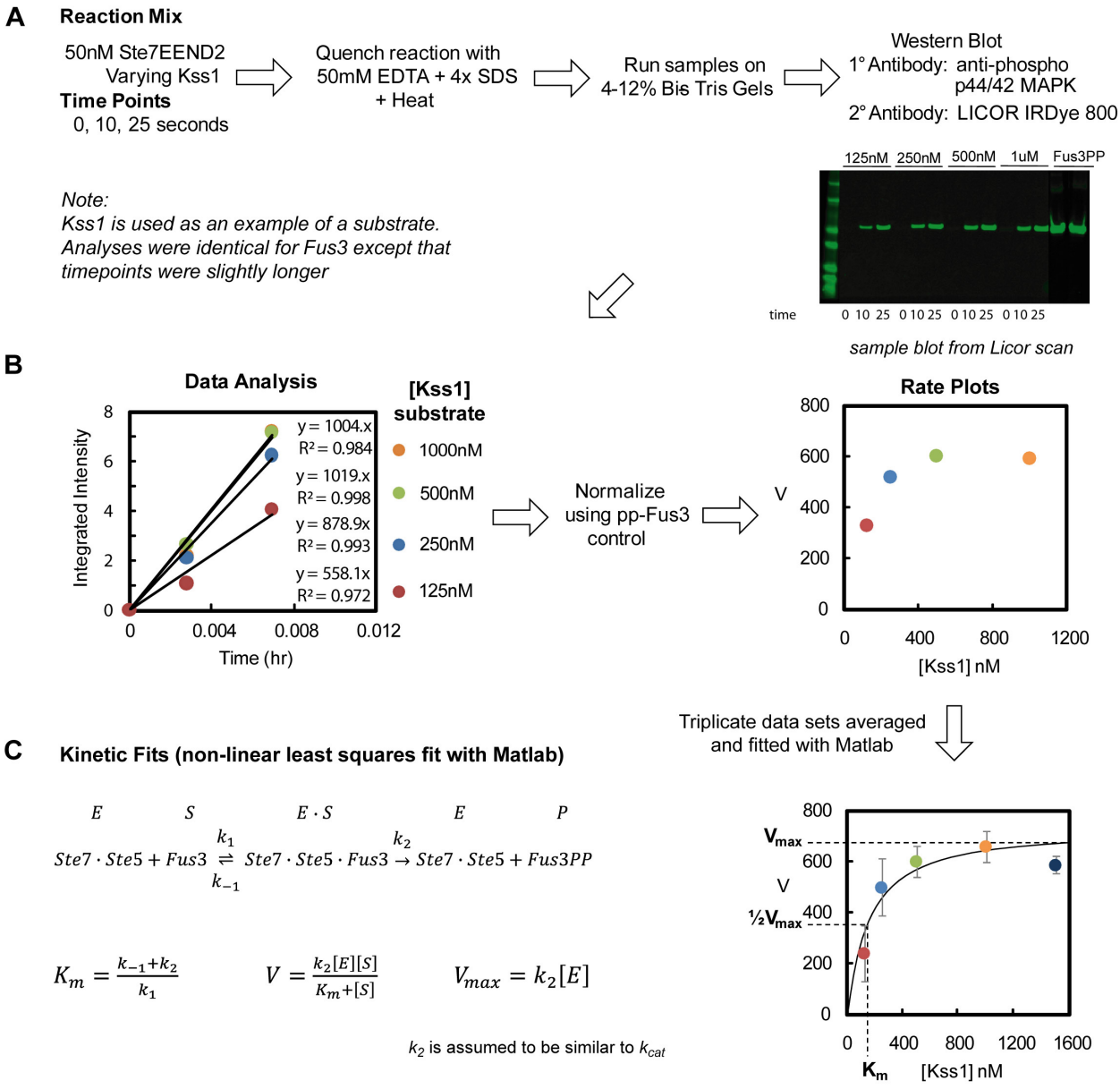

Supp. 4: (A) Reaction setup for anti-phospho MAPK western: reactions contain 50nM enzyme (Ste7EE-ND2) and varying amount of subtrate (Fus3 or Kss1); various timepoints were taken and then run on gels and transferred to nitrocellulose. Primary antibody is an anti-phospho p44/42 MAPK antibody (Cell Signaling Technology #9101), and secondary is an IRDYE 800CW goat anti-rabbit IgG antibody (Licor). (B) Blots were scanned on Licor Odyssey Imaging System and data was analyzed using Odyssey 2.1 software to generate rate plots (using initial rates). (C) Triplicate data sets were fit to the Michaelis-Menten equation with Matlab to calculate K_M and k_{cat} for each curve. Error bars represent standard deviation of the values from three independent experiments.

Supplemental Figure 5 - Structure of Ste5-ms and homology to other VWA domains

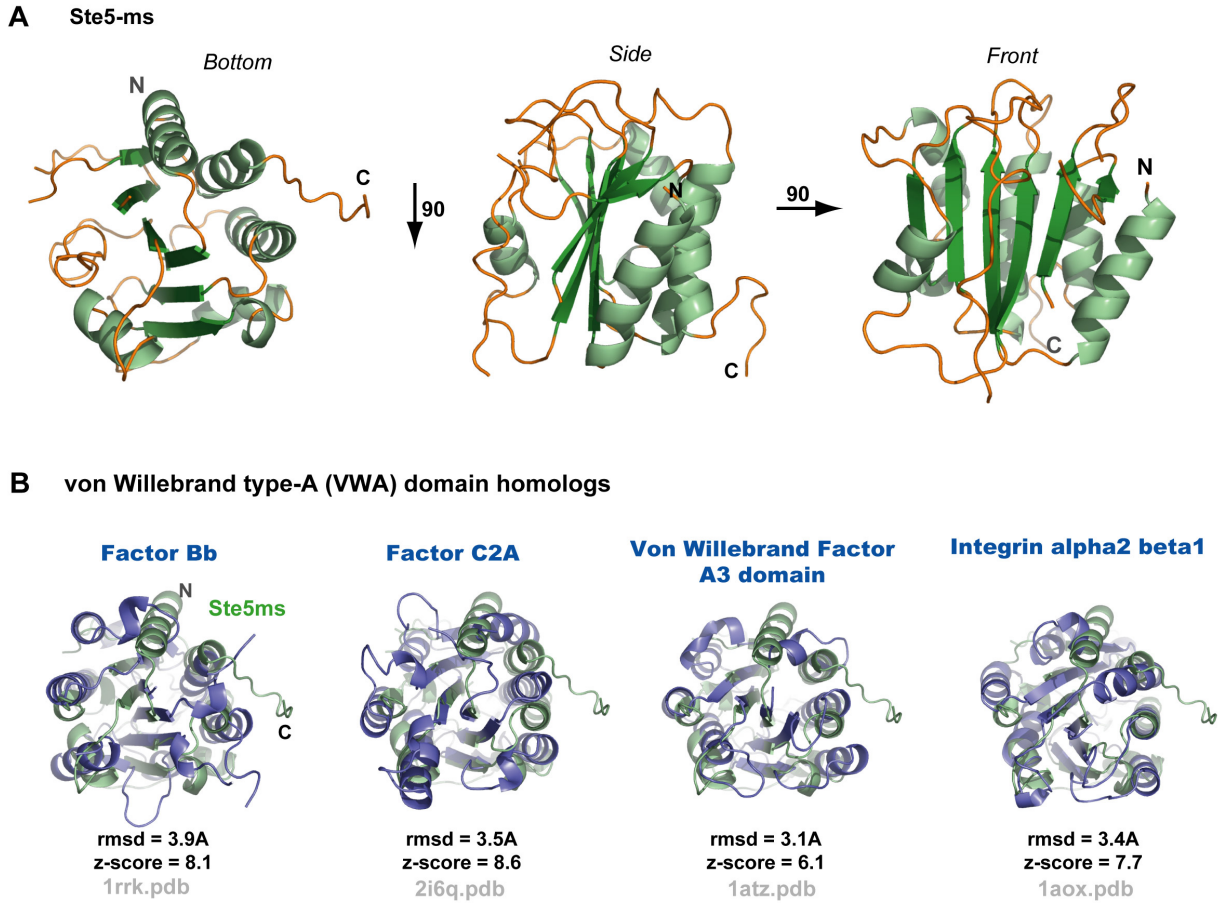

Supp. 5: (A) 1.6 angstrom crystal structure of Ste5-ms. For crystallographic statistics, see Supp. Table 2. (B) Ste5-ms is structurally homologous (but not related by primary sequence) to the von Willebrand type-A (VWA) domain. Alignment to the VWA of various proteins (Factor Bb and C2A of the complement system, and Integrin LFA-1 domain) using DALI server. Rmsd is root-mean squared deviation.

Conclusion: Ste5-ms is a folded domain homologous to the VWA domain found in a number of other proteins

Supplemental Figure 6 - Testing activity of Ste5-ms surface mutants

A **Distribution of surface mutants on Ste5-ms (593-786)**

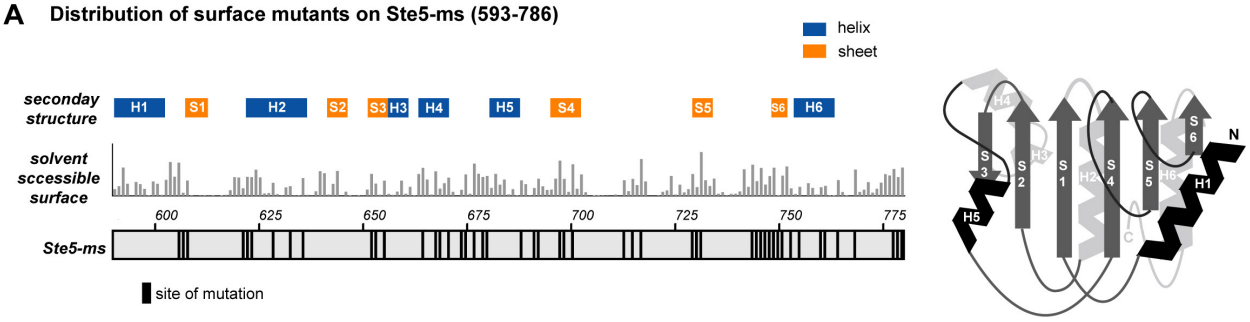

B **Ability of Ste5-ms mutants to co-catalyze Ste7-Fus3 phoshorylation**

Ste5-ms mutant	Mutated Residues
wild-type	none
1	K606A, P607A, D608A
2	L621A, K622A, E623A
3	I628A, N632A, K635A
4	R651A, N652A, Y754A
5	H663A, D666A, S667A
6	D669A, S672A, N673A
7	K675A, K677A, S678A
8	I686A, K689A, N690A
9	E695A, N696A, H698A
10	N710A, E712A, K714A
11	T726A, S727A, F728A
12	R731A, R732A, P733A
14	V745A, Y747A, S748A
15	K750A, I751A, D752A
16	N744A, D746A
17	L754A, E756A
18	T761A, F762A
19	E765A, Y769A
593-777	deletion of 778-786
no Ste5ms	na

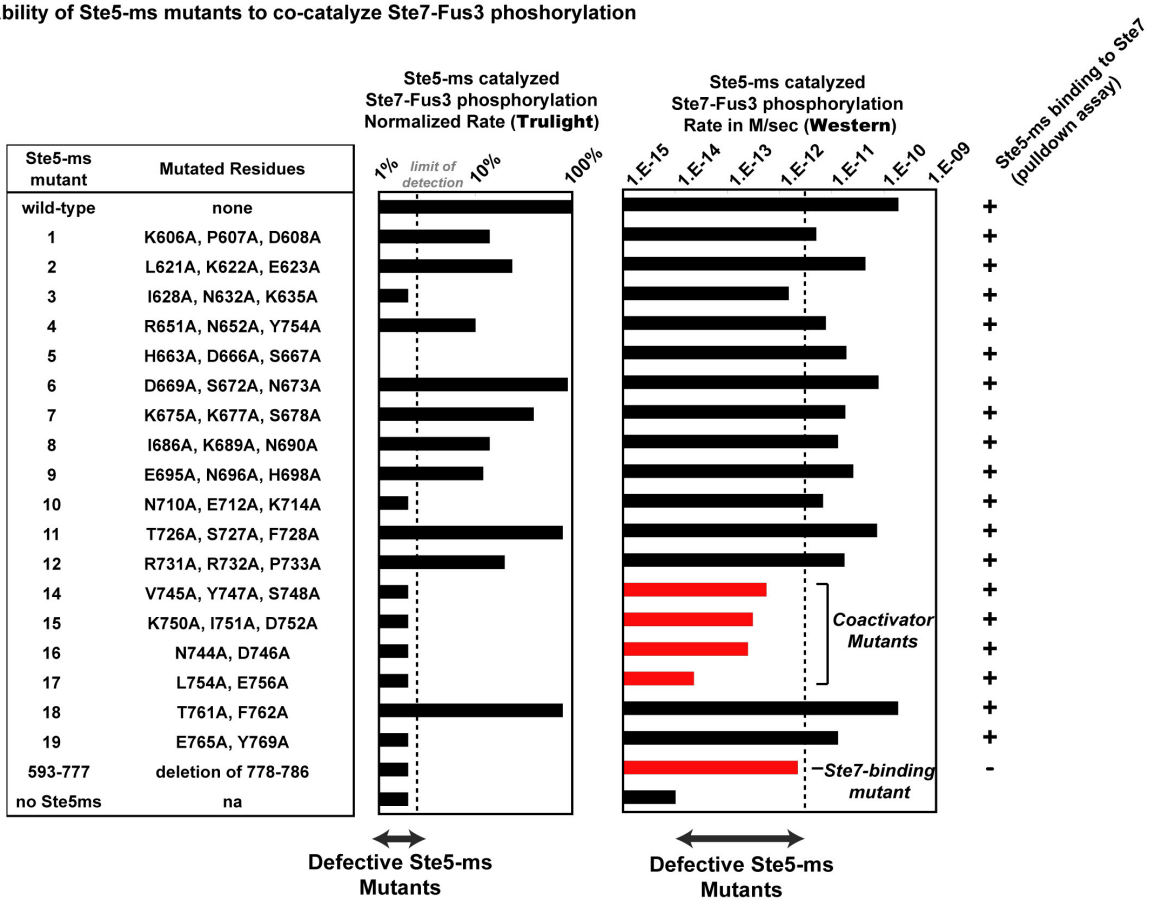

Supp. 6: (A) Positions of Ste5-ms surface mutants along primary sequence of ms domain. Secondary structure and solvent accessible surface (SAS) are also shown. Topology model of Ste5-ms is displayed on the right. (B) Table of Ste5-ms mutants summarizing ability to co-catalyze Ste7-to-Fus3 phosphorylation - measured by the Trulight and anti-phospho MAPK western blot assays (reactions contained 50nM Ste7EE-ND2, 1uM Fus3-K42R, and 1uM MBP-Ste5-ms variant). Defective Ste5-ms mutants are defined as falling below the limit of detection of the Trulight assay (or about 100-fold less activity than wild-type Ste5-ms). Ability of Ste5-ms variants to bind to GST-Ste7wt in pulldown assays is shown to the right. Red bars indicate mutations that cluster on two interfaces on the surface of Ste5-ms and that are examined in detail in the main figures and text.

Supplemental Figure 7 - Distinct Ste5-ms surface mutants affect Ste7-binding or catalysis

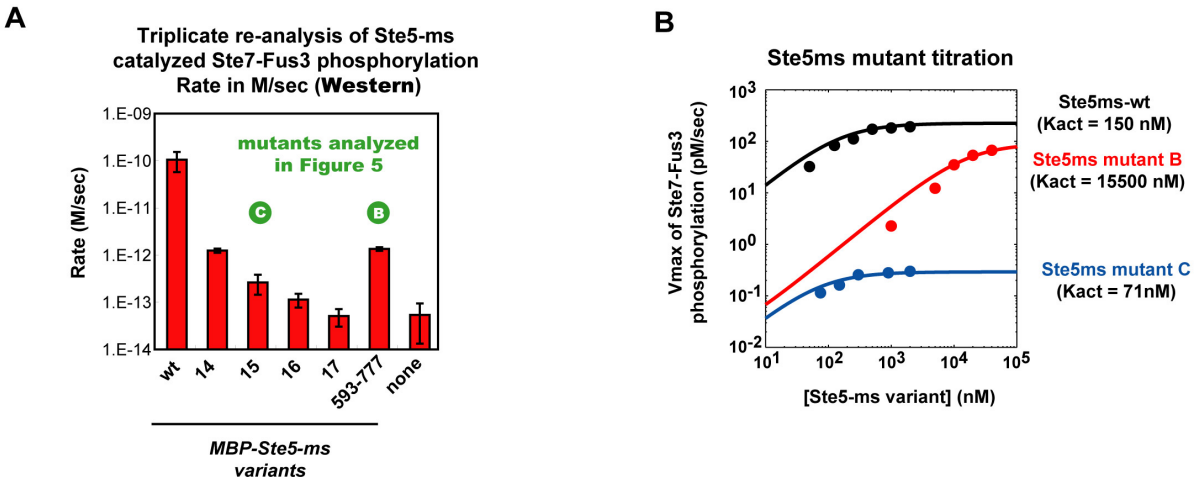

Supp. 7: (A) The most defective Ste5-ms mutants (MBP-fused) were re-tested in for ability to promote Ste7-Fus3 phosphorylation using anti-phospho MAPK western blot kinase assay (reactions contained 50nM Ste7EE-ND2, 1uM Fus3-K42R, and 1uM MBP-Ste5-ms variant). Representative Ste5-ms mutants 'B' and 'C', highlighted extensively in main Figure 5, are denoted by green balls. (B) Log-log plot of titration of Ste5-ms mutants versus Vmax for Ste7-Fus3 phosphorylation (50nM Ste7EE-ND2, 1uM Fus3-K42R and variable concentration of MBP-Ste5-ms variant: 50nM to 40000nM). The activity Ste5-ms mutant 'B' can be restored to near wild-type levels by increasing it's concentration (from 1uM to 60uM). Ste5-ms Mutant 'C' has a $K_{activation}$ near Ste5-ms wildtype (~70nM versus 150nM for wild-type) but is crippled in its ability to co-catalyze Fus3 phosphorylation by Ste7EE-ND2. $K_{activation}$ of Ste5-ms mutant 'B' is ~ 15500 nM.

Conclusion: Ste5-ms has two functionally distinct surfaces important for: kinase binding (to Ste7) and co-catalysis of Ste7-Fus3 phosphorylation

Supplemental Figure 8 - Identification of Fus3 mutants that increase phosphorylation by Ste7 in the absence of the Ste5 scaffold

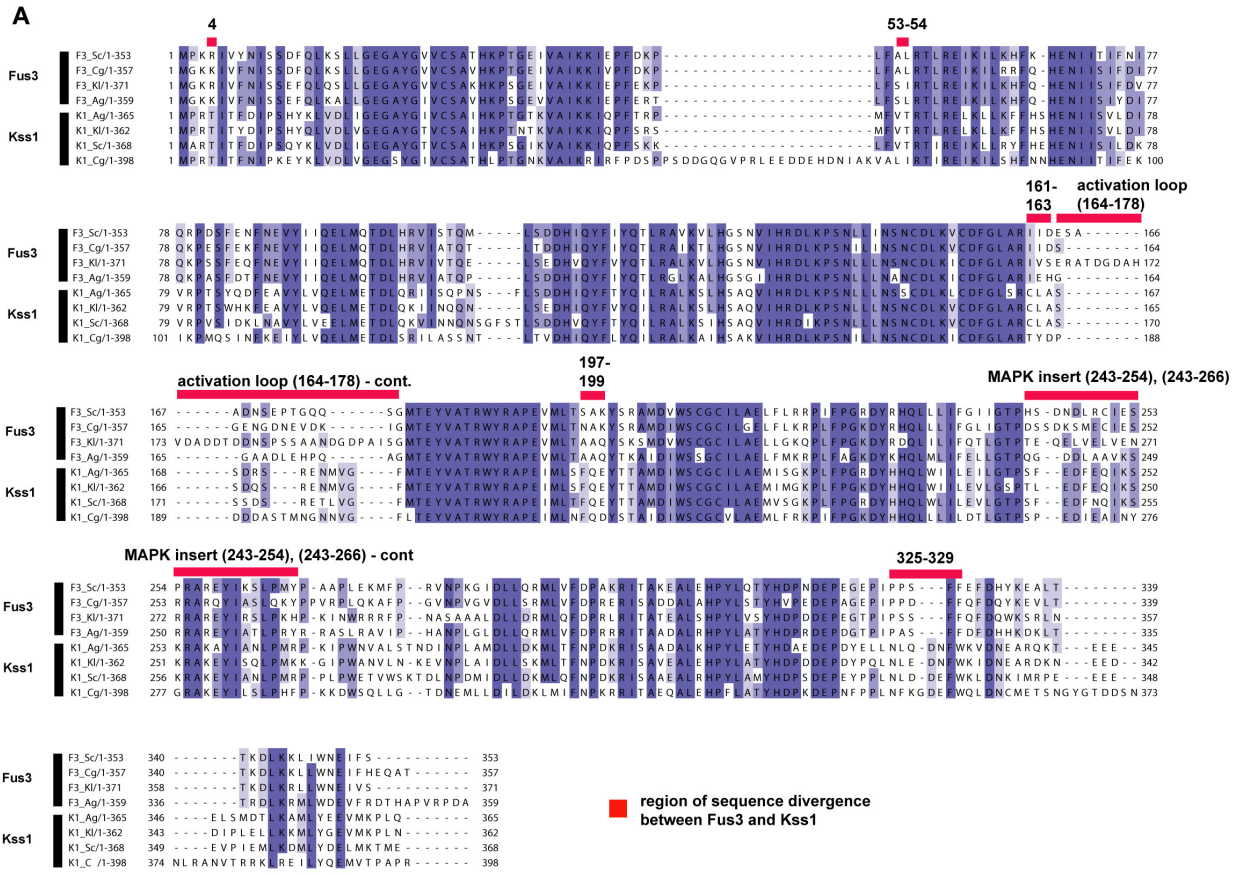

B **List of Fus3 mutations**

Fus3 mutants	Region on Fus3 Mutated Out	Fus3 sequence	Region of Kss1 Swapped In	Kss1 sequence
1	4	R	4	T
2	53-53	AL	53-54	VI
3,4	161	I	167	C or L
5	161-163	IID	167-169	CLA
6	164-178	ESAADNSEPTGQQSG	170-181	SSSDSRETLVGF
7	197-199	SAK	200-202	FQE
8	243-254	HSDNDLRCIESP	246-256	SFEDFNQIKSK
9	243-266	HSDNDLRCIESPRAREYIKSLPMY	246-268	SFEDFNQIKSKRAKEYIANLPMR
10	325-329	PPSFF	329-335	NLDDEFW

Supp. 8: (A) Alignment of Fus3 and Kss1 homologs from four yeast species (*S.cer, A.gos, C.gla, and K.lac*). Regions of high conservation are shaded purple. Positions differing between the two subgroups (Fus3 and Kss1 subfamilies) and not part of the core of the kinase domain were chosen for making chimeric mutations in Fus3 using the corresponding region from Kss1. Mutations were generated in functional blocks (red bars) rather than individually. (B) List of Fus3 mutations and amino acid sequence of swapped regions. Note, some larger chimeric genes were constructed, but the encoded proteins were unstable and did not express (including 197-199, and N- and C-lobe swaps: 161-353, and 1-160).

Supplemental Figure 8 (Continued) - Identification of Fus3 mutants that increase phosphorylation by Ste7 in the absence of the Ste5 scaffold

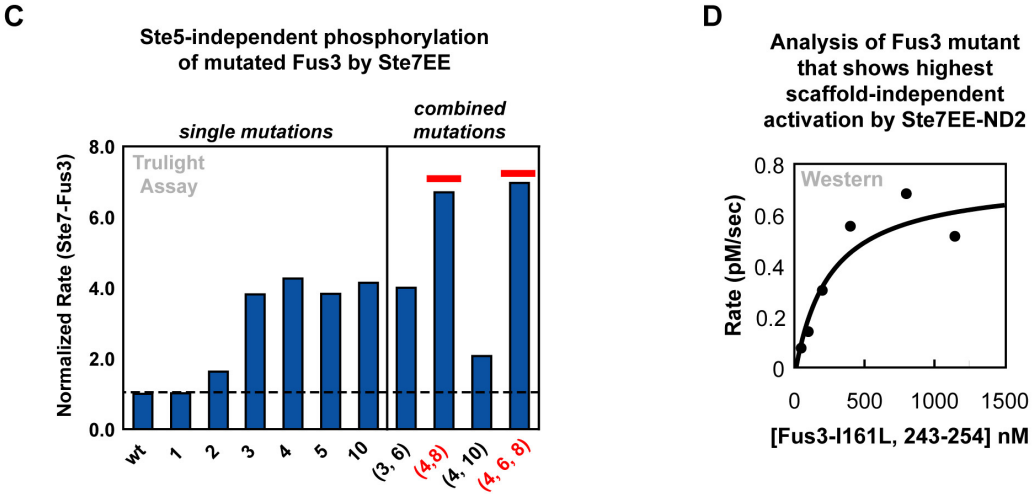

Supp. 8 (cont.): (C) Testing Ste5-independent Fus3 mutant activation by Ste7EE-ND2 alone with the Trulight kinase assay (50nM each component). Fus3 mutations are described in Supp. Fig. 8 panel B. We found that many Fus3 chimeric mutants had high levels of autophosphorylation when purified from *E. coli*, which confounded our analysis. Therefore, we re-expressed these Fus3 mutants (all except 1, 2, 9) with lambda phophatase so they would be dephosphorylated for our assays. Fus3 mutants most-easily activated by Ste7EE in the absence of Ste5-ms are noted in red. Not all mutant variants of Fus3 could be expressed - a number of combined mutations made the protein insoluble. (D) The Fus3 double mutant (I161L, 243-254) can be activated much better than Fus3-wt, in the absence of Ste5-ms. Rate plot of Ste5-independent phosphorylation of mutated Fus3 (I161L, 243-254) by 50nM Ste7EE-ND2, determined by anti-phospho MAPK western, shows that this Fus3 mutant can be phosphorylated by Ste7 approximately 20-fold more rapidly than Fus3-wt.

Conclusion: Mutations can unlock Fus3 for Ste5-independent phosphorylation by Ste7

Supplemental Figure 9: ERK duplication and emergence of Ste5 scaffold in Saccharomycotina

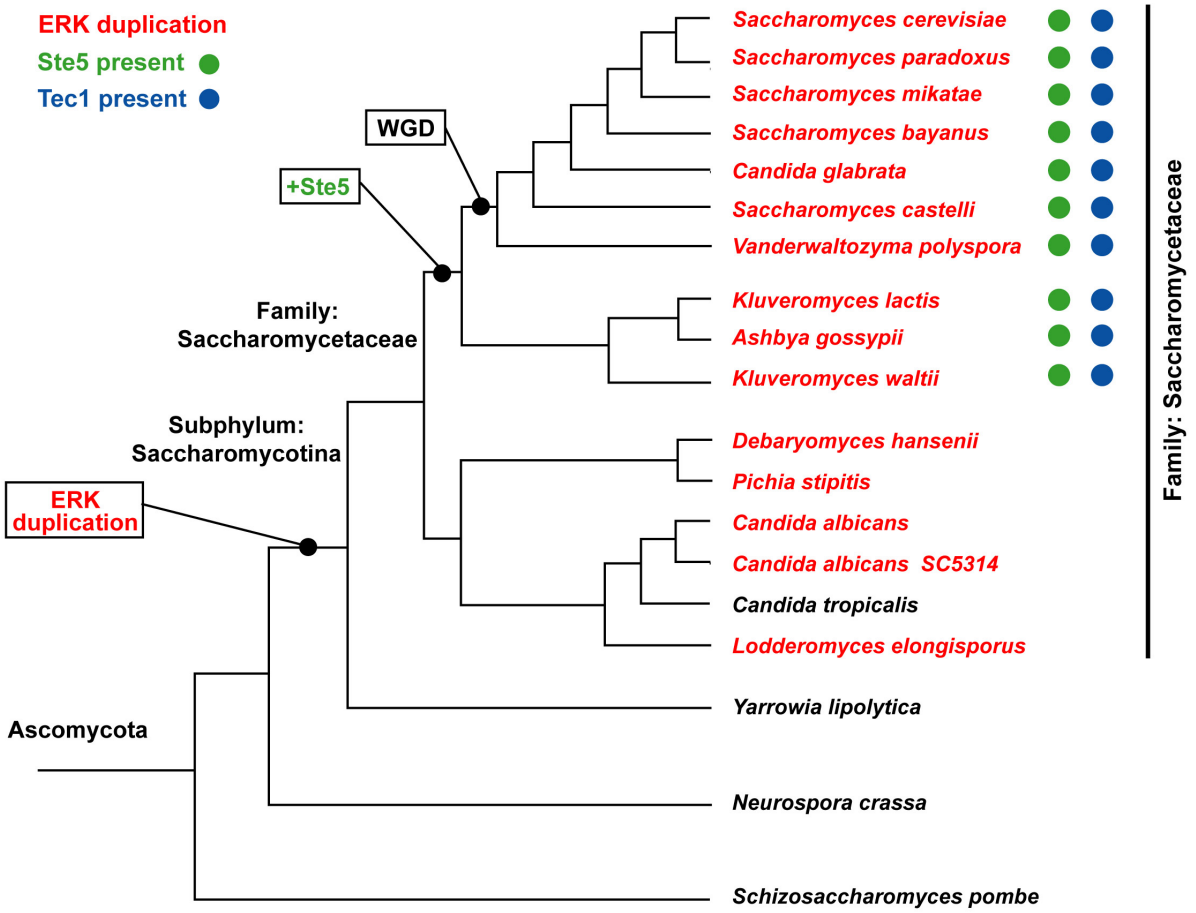

Supp. 9: Fungal phylogenetic tree adapted from Wapinski et. al fungal whole genome duplication (WGD) paper (Wapinski, 2007). Other fungal genomes found to contain an ERK duplication, not in the Wapinski tree, were added as branches. Phylogeny was reconstructed using other reports to infer relationships not seen in Wapinski paper. Kurtzman et. al paper places *Vanderwaltozyme polysporus* (aka *K.* or *V. polysporus*) next to *Candida glabrata* (Kurtzman, 2003). Scannell et. al paper puts *V. polypora* within WGD set but furthest from *S.cer* (Scannell, 2007). Tsui et. al paper groups all clinically relevant *Candida* species (including *P. stipitis* next to *D. hansenii*, and *L. elongisporus* next to *C. tropicalis*) (Tsui, 2008). Tree branch distances are arbitrary. All ERK duplications occur in the family saccharomycetaceae. Ste5 does not cluster by whole genome duplication (WGD) or genus. Genomes with Ste5 scaffold homologs have a green dot. Genomes with Tec1 homologs have a blue dot.

Conclusion: Fus3/Kss1 (ERK-family) duplication and divergence occurs within the subphylum Saccharomycotina and covaries with the presence of the Ste5 scaffold and the Tec1 transcription factor.

Table S1. Constructs used in this study

Plasmid	Parent Vector	Gene	N-term. fusion	C-term. fusion	Expression System
vMG500	pBH4	Fus3wt	TEV cleavable His6		E. coli
vMG510	pBH4	Fus3-K42R	TEV cleavable His6		E. coli
vMG515	pBH4	Fus3-K42R-(I161L, 243-254)	TEV cleavable His6		E. coli
vMG530	vMG950	Fus3wt	TEV cleavable His6		E. coli
vMG531	vMG950	Fus3-I161C	TEV cleavable His6		E. coli
vMG532	vMG950	Fus3-I161L	TEV cleavable His6		E. coli
vMG533	vMG950	Fus3-(161-163)	TEV cleavable His6		E. coli
vMG534	vMG950	Fus3-(325-329)	TEV cleavable His6		E. coli
vMG540	vMG950	Fus3-(I161L, 243-254)	TEV cleavable His6		E. coli
vMG541	vMG950	Fus3-(I161L, 325-329)	TEV cleavable His6		E. coli
vMG542	vMG950	Fus3-(I161L, 164-178, 243-254)	TEV cleavable His6		E. coli
vMG543	vMG950	Fus3-(161-163, 243-254)	TEV cleavable His6		E. coli
vMG544	vMG950	Fus3-(161-163, 325-329)	TEV cleavable His6		E. coli
vMG550	vMG950	Fus3/Kss1	TEV cleavable His6		E. coli
vMG551	vMG950	Kss1/Fus3	TEV cleavable His6		E. coli
vMG800	pFBHt-b	Kss1	TEV cleavable His6		SF9
vMG600	pFB1MG	Ste7wt	TEV cleavable GST	His6	SF9
vMG610	pFB1MG	Ste7EE	TEV cleavable GST	His6	SF9
vMG612	pFB1MG	Ste7EE-ND2	TEV cleavable GST	His6	SF9
vMG613	pFB1MG	Ste7EE-ND1/2	TEV cleavable GST	His6	SF9
vMG700	pBH4	Ste5-ms	TEV cleavable His6		E. coli
vMG705	pBH4	KCK-Ste5ms (C724A)	TEV cleavable His6		E. coli
vMG720	pETARA	ΔN-Ste5	TEV cleavable GST	His6	E. coli
vMG711	pETARA	ΔN-Ste5-ND	TEV cleavable GST	His6	E. coli
vMG721	pETARA	Ste5 (316-916)	TEV cleavable GST	His6	E. coli
vMG723	pETARA	Ste5 (518-916)	TEV cleavable GST	His6	E. coli
vMG724	pETARA	Ste5 (691-916)	TEV cleavable GST	His6	E. coli
vMG726	pETARA	Ste5 (280-750)	TEV cleavable GST	His6	E. coli
vMG733	pETARA	Ste5 (518-851)	TEV cleavable GST	His6	E. coli
vMG734	pETARA	Ste5 (518-786)	TEV cleavable GST	His6	E. coli
vMG735	pETARA	Ste5 (518-777)	TEV cleavable GST	His6	E. coli
vMG738	pETARA	Ste5 (583-786)	TEV cleavable GST	His6	E. coli
vMG739	pETARA	Ste5 (593-786)	TEV cleavable GST	His6	E. coli
vMG750-vMG770	pETARA	Ste5-ms (mutant variants) [21 variants]	TEV cleavable GST	His6	E. coli
vMG775 vMG795	pMBP	Ste5-ms (mutant variants) [21 variants]	TEV cleavable MBP	His6	E. coli

pBH4 is a pET derived bacterial expression vector that makes your protein with a TEV-cleavable N-terminal His6 fusion

VMG950 is a vector for bicistronic expression of gene of interest with GST-lambda phosphatase (gene is expressed with a TEV-cleavable N-terminal His6 tag)

pETARA is a pET derived bacterial expression that makes your protein with a TEV-cleavable N-terminal GST fusion and C-terminal His6 fusion

pMBP is a pET derived bacterial expression that makes your protein with a TEV-cleavable N-terminal MBP fusion and C-terminal His6 fusion

pFBHt-b is a shuttle vector (pFastbac-Ht-b, Invitrogen) for SF9 expression that makes your protein with a TEV-cleavable N-terminal His6 fusion

pFB1MG is modified pFastbac1 vector (Invitrogen) for SF9 expression that makes your protein with a TEV-cleavable N-terminal GST fusion and C-terminal His6

* numbers for Fus3 genes denote regions swapped with Kss1 sequence

Table S2. Crystallographic Statistics

		$HgCl_2$		
Data Statistics	**native**	λ1 (peak)	λ2 (inflection)	λ3 (remote)
Space Group	$P2_12_12_1$	$P2_12_12_1$		
Cell	46.8, 63.6, 69.1, 90, 90, 90	45.9, 63.2, 68.9, 90, 90, 90		
Wavelength	1.11587 Å	1.00556 Å	1.00949 Å	1.04796 Å
Resolution (last shell)	50-1.6Å (1.66-1.60Å)	50-2.1Å (2.18-2.10Å)	50-2.1Å (2.18-2.10Å)	50-2.1Å (2.18-2.10Å)
Unique Reflections	25696	12160	12123	12128
Redundancy	4.3 (3.9)	7.4 (7.4)	5.2 (5.1)	7.5 (7.4)
Completeness	92.4% (93.9%)	99.8% (99.8%)	99.7% (100%)	99.8% (99.8%)
I/σ	19.3 (4.0)	20.8 (5.0)	18.1 (4.4)	20.8 (5.0)
R_{sym}	0.046 (0.311)	0.07 (0.326)	0.056 (0.334)	0.058 (0.357)
Mean Figure of Merit		0.563; 0.75 after solvent flattening		
Refinement Statistics				
Resolution Range	22.17 - 1.60			
Reflections Used Work (Test)	24227 (1224)			
R_{cryst}/R_{free}	0.209 / 0.237			
Overall Figure of Merit	0.845			
r.m.s.d. bonds/angles	0.005Å / 0.952°			
Average B factor	29.91Å2			
Overall B_{wilson}	20.23Å^2			
Ramachandran Analysis (Preferred / Allowed)	94.4.% / 4.2%			

r.m.s.d. is the root-mean squared deviation from ideal geometry

$R_{sym} = \Sigma_{hkl}\Sigma_i |I_{hkl,i} - \langle I_{hkl,i}\rangle| / \Sigma_{hkl}\Sigma_i |I_{hkl,i}|$

R_{cyst} and $R_{free} = \Sigma||F_{obs} - F_{calc}||/\Sigma|F_{obs}|$. F_{obs} and F_{calc} are observed and calculated structure factors. R_{free} is calculated from a set of randomly chosen 5% of reflections, and R_{cyst} is calculated with the remaining 95% of reflections.

SUPPLEMENTAL REFERENCES

Adams, P. D., Grosse-Kunstleve, R. W., Hung, L. W., Ioerger, T. R., McCoy, A. J., Moriarty, N. W., Read, R. J., Sacchettini, J. C., Sauter, N. K., and Terwilliger, T. C. (2002). PHENIX: building new software for automated crystallographic structure determination. Acta Crystallogr D Biol Crystallogr *58*, 1948-1954.

Emsley, P., and Cowtan, K. (2004). Coot: model-building tools for molecular graphics. Acta Crystallogr D Biol Crystallogr *60*, 2126-2132.

Kurtzman, C. P. (2003). Phylogenetic circumscription of Saccharomyces, Kluyveromyces and other members of the Saccharomycetaceae, and the proposal of the new genera Lachancea, Nakaseomyces, Naumovia, Vanderwaltozyma and Zygotorulaspora. FEMS Yeast Res *4*, 233-245.

Morris, R. J., Perrakis, A., and Lamzin, V. S. (2003). ARP/wARP and automatic interpretation of protein electron density maps. Methods Enzymol *374*, 229-244.

Murshudov, G. N., Vagin, A. A., and Dodson, E. J. (1997). Refinement of macromolecular structures by the maximum-likelihood method. Acta Crystallogr D Biol Crystallogr *53*, 240-255.

Otwinowski, Z., and Minor, W. (1997). Processing of X-ray Diffraction Data Collected in Oscillation Mode. In Macromolecular Crystallography, Part A, J. N. Abelson, M. I. Simon, C. W. Carter Jr., and R. M. Sweet, eds. (Academic Press), pp. 307-326.

Remenyi, A., Good, M. C., Bhattacharyya, R. P., and Lim, W. A. (2005). The role of docking interactions in mediating signaling input, output, and discrimination in the yeast MAPK network. Mol Cell *20*, 951-962.

Scannell, D. R., Frank, A. C., Conant, G. C., Byrne, K. P., Woolfit, M., and Wolfe, K. H. (2007). Independent sorting-out of thousands of duplicated gene pairs in two yeast species descended from a whole-genome duplication. Proc Natl Acad Sci U S A 104, 8397-8402.

Terwilliger, T. C. (2003). Automated main-chain model building by template matching and iterative fragment extension. Acta Crystallogr D Biol Crystallogr *59*, 38-44.

Terwilliger, T. C., and Berendzen, J. (1999). Automated MAD and MIR structure solution. Acta Crystallogr D Biol Crystallogr *55*, 849-861.

Tsui, C. K., Daniel, H. M., Robert, V., and Meyer, W. (2008). Re-examining the phylogeny of clinically relevant Candida species and allied genera based on multigene analyses. FEMS Yeast Res *8*, 651-659.

Wapinski, I., Pfeffer, A., Friedman, N., and Regev, A. (2007). Natural history and evolutionary principles of gene duplication in fungi. Nature *449*, 54-61.